Dynamical lattice models for binary alloys under irradiation: Mean-field solutions and Monte Carlo simulations

E. Salomons,* P. Bellon, F. Soisson, and G. Martin
CEREM-DTM-SRMP, CEN Saclay, 91191 Gif-sur-Yvette CEDEX, France
(Received 7 October 1991)

Ordering in binary bcc alloys under irradiation is studied using dynamical nearest-neighbor lattice models. Steady-state mean-field solutions (point and pair approximation) and Monte Carlo simulations are presented. Both for a model with a direct-exchange transport mechanism and for a model with a vacancy transport mechanism, it is found that the $A2$-$B2$ ordering transition becomes first order beyond a tricritical point (i.e., at high radiation flux). The effect of replacement collision sequences, induced by high-energy radiation, is also investigated.

I. INTRODUCTION

Order-disorder phenomena in binary alloys are expected to be affected by energetic-particle irradiation. This can be understood from the fact that energetic particles collide with atoms in the alloy, and displace them from their equilibrium positions. As a consequence, atomic transport (and hence disorder) increases under radiation: vacancy migration is enhanced, and moreover high-energy radiation produces replacement collision sequences, i.e., displacements of rows of atoms.[1-3]

To study the statistical mechanics of binary alloys one can use the equivalent of the Ising model: A and B atoms occupying the sites of a rigid lattice, with pair interactions between atoms at nearest-neighbor sites. The usual method of solving this model starts from the Ising Hamiltonian, and yields the free energy and other thermodynamic quantities through a mean-field approximation. An alternative route starts from the dynamics of the atoms (e.g., one can assume that atoms perform thermally activated exchanges between nearest-neighbor sites), and yields thermodynamic properties as steady-state solutions of mean-field rate equations. Instead of solving mean-field rate equations, one can also perform Monte Carlo simulations of the dynamics of the system.

The advantage of a description in terms of the dynamics is that radiation-induced atomic displacements can be implemented in the model (it is not clear how these can be implemented in a Hamiltonian description, except in simple cases[4]). Thus, the nonequilibrium statistical mechanics of binary alloys under radiation can be studied by dynamical lattice models with radiation-induced transport in addition to thermal transport. In this paper we discuss solutions of such models for the $B2$ (β-brass) structure, obtained by mean-field approximations and Monte Carlo simulation. A complete model for high-energy irradiation includes: thermally activated atomic jumps (via a vacancy mechanism and/or an interstitial mechanism), radiation-induced direct exchanges of two or more atoms, and also radiation-induced atom-vacancy exchanges due to secondary projectiles.[5] Here we ignore interstitials and we restrict ourselves to models with a single transport mechanism, either a direct-exchange or a vacancy mechanism. The model with a vacancy mechanism is expected to be a realistic representation of an alloy under subthreshold radiation, i.e., radiation with an energy too low to induce direct displacements of atoms. The model with a direct-exchange mechanism has been studied previously in the point approximation by Bellon and Martin[6] and through simulations by Haider.[7] Other studies of Ising models with competing dynamics have been reported in Refs. 8–13.

In Sec. II we study a model for a binary alloy without vacancies, with a direct-exchange mechanism for both thermal and radiation-induced transport. In Sec. III we extend this to the case where replacement collision sequences occur. In Sec. IV we study a model for a binary alloy with vacancies (i.e., a ternary system), with a vacancy mechanism for both thermal and radiation-induced transport.

II. RADIATION-INDUCED DIRECT NEAREST-NEIGHBOR EXCHANGES

A. Model system

The system consists of a bcc lattice with $\frac{1}{2}N$ α sites and $\frac{1}{2}N$ β sites. Each site is occupied by either an A atom or a B atom. Nearest-neighbor pair interactions are denoted by V_{AA}, V_{BB} and V_{AB}, and the ordering energy is defined as $\omega = V_{AA}+V_{BB}-2V_{AB}$. The total energy of the model system is given by a sum over nearest-neighbor pairs:

$$E^{\rm tot} = \sum_{i<j} V_{ij} \quad (i,j=A,B) \tag{1}$$

(e.g., if site i is occupied by an A atom, and site j by a B atom, then $V_{ij}=V_{AB}$). We use the notation of Muto and Takagi[14] (the symbol A_α indicates an A atom at an α site):

$$R_\alpha \tfrac{1}{2}N = c(1+S)\tfrac{1}{2}N:\ \text{total number of } A_\alpha \text{ atoms},$$
$$R_\beta \tfrac{1}{2}N = [1-c(1-S)]\tfrac{1}{2}N:\ \text{total number of } B_\beta \text{ atoms},$$
$$W_\alpha \tfrac{1}{2}N = [1-c(1+S)]\tfrac{1}{2}N:\ \text{total number of } B_\alpha \text{ atoms},$$
$$W_\beta \tfrac{1}{2}N = c(1-S)\tfrac{1}{2}N:\ \text{total number of } A_\beta \text{ atoms}, \tag{2}$$

where c is the average concentration of A atoms in the lattice (average number of A atoms per site), and S is the long-range order parameter. Further:

$$Q_{AA}\tfrac{1}{2}N = Q\tfrac{1}{2}N:\ \text{total number of } A_\alpha\text{-}A_\beta \text{ pairs},$$
$$Q_{AB}\tfrac{1}{2}N = (zR_\alpha - Q)\tfrac{1}{2}N:\ \text{total number of } A_\alpha\text{-}B_\beta \text{ pairs},$$
$$Q_{BA}\tfrac{1}{2}N = (zW_\beta - Q)\tfrac{1}{2}N:\ \text{total number of } B_\alpha\text{-}A_\beta \text{ pairs},$$
$$Q_{BB}\tfrac{1}{2}N = [z(W_\alpha - W_\beta)+Q]\tfrac{1}{2}N:\ \text{total number of } B_\alpha\text{-}B_\beta \text{ pairs}, \tag{3}$$

where z is the coordination number of the lattice ($z=8$ for bcc), and the symbol A_α-B_β indicates a nearest-neighbor pair of an A_α and a B_β atom. Note that these relations satisfy $Q_{AA}+Q_{AB}=zR_\alpha$, $Q_{BA}+Q_{BB}=zW_\alpha$, $Q_{AA}+Q_{AB}+Q_{BA}+Q_{BB}=z$, as required.

B. Dynamics

We assume that the dynamics of the system is governed by nearest-neighbor A-B exchanges.

1. System in equilibrium

In a system in equilibrium at temperature T, A-B exchanges are thermally activated. A microscopic configuration of the system is denoted by X. For the probability per unit time that the system makes a transition to configuration X', we use the function

$$W(X\to X') = \nu \exp\left[-\frac{E_s^{\text{tot}}-E_x^{\text{tot}}}{kT}\right], \tag{4}$$

where ν is a constant frequency, E_x^{tot} is the total energy in configuration X, and the "saddle-point" energy E_s^{tot} is a constant, independent of the states X and X'. The function $W(X\to X')$ satisfies detailed balance

$$W(X\to X')P_{\text{eq}}(X) = W(X'\to X)P_{\text{eq}}(X'), \tag{5}$$

where $P_{\text{eq}}(X)$ is the probability density in configuration space. Since we are dealing only with nearest-neighbor interactions, we can write expression (4) for a single A-B exchange as

$$W(A_iB_j\to B_iA_j) = \nu \exp\left[-\frac{E_s - \sum_{i'} V_{ii'} - \sum_{j'} V_{jj'}}{kT}\right], \tag{6}$$

where i' and j' denote nearest-neighbor sites of site i and site j, respectively, and E_s is a constant. As site i and site j are nearest-neighbors of each other, the i-j interaction is counted double in (6), but since only A-B exchanges are considered, this yields a constant term $-2V_{AB}$. As we want to use the transition probability (6) in Monte Carlo simulations, we choose $E_s=(z-1)(V_{AA}+V_{BB})+2V_{AB}$, so that the argument of the exponential function is always negative (or zero), and the energy barrier for a thermally activated exchange is always positive (or zero).

2. System under radiation

In a system under radiation, we assume that both thermally activated exchanges and ballistic exchanges occur. This means, that we model the effect of a radiation flux as forced exchanges of nearest-neighbor atoms, independent of the temperature and the atomic configuration.[6] The transition probability per unit time now becomes

$$W(A_iB_j\to B_iA_j) = \nu\left[r+(1-r)\exp\left[-\frac{E_s - \sum_{i'} V_{ii'} - \sum_{j'} V_{jj'}}{kT}\right]\right], \tag{7}$$

where r is a measure of the radiation flux ($0\le r\le 1$). The physical meaning of this expression is that a transition is a ballistic exchange with probability r and a thermal-exchange attempt with probability $(1-r)$. The ballistic-exchange frequency is $\Gamma_b=\nu r$ and the thermal-exchange attempt frequency is $\Gamma_t=\nu(1-r)$. In the following, we choose the unit of time as $\tau=1/\nu$, i.e., we set $\nu=1$.

C. Mean-field solutions

In this section the model described above is solved in the Bragg-Williams approximation (or point approximation) and in the pair approximation.

1. Bragg-Williams approximation

In the Bragg-Williams approximation a microscopic configuration of the system described in Sec. II A is specified by a single parameter: the long-range order parameter S [see Eq. (2)]. We define $\Gamma_{\alpha\beta}$ and $\Gamma_{\beta\alpha}$ as the average exchange frequencies of A_α-B_β and B_α-A_β pairs, respectively. In the Bragg-Williams approximation one can write the following rate equation for the total number $R_\alpha \frac{1}{2} N$ of A_α atoms:

$$\frac{d(R_\alpha \frac{1}{2}N)}{dt} = -\Gamma_{\alpha\beta} R_\alpha R_\beta + \Gamma_{\beta\alpha} W_\beta W_\alpha . \quad (8)$$

The steady-state solution of this equation is

$$\frac{R_\alpha R_\beta}{W_\beta W_\alpha} = \frac{\Gamma_{\beta\alpha}}{\Gamma_{\alpha\beta}} \quad (9)$$

or

$$\frac{1-c+S+cS^2}{1-c-S+cS^2} = \frac{\Gamma_{\beta\alpha}}{\Gamma_{\alpha\beta}} . \quad (10)$$

To evaluate $\Gamma_{\beta\alpha}/\Gamma_{\alpha\beta}$ we make the following approximation in Eq. (7):

$$\sum_{i'} V_{ii'} + \sum_{j'} V_{jj'} = z[W_\beta V_{AA} + R_\beta V_{AB} + W_\alpha V_{BB} + R_\alpha V_{AB}] = z[-cS\omega + cV_{AA} + (1-c)V_{BB} + V_{AB}]$$

$$\text{for an } A_\alpha\text{-}B_\beta \text{ exchange} , \quad (11a)$$

$$\sum_{i'} V_{ii'} + \sum_{j'} V_{jj'} = z[W_\beta V_{AB} + R_\beta V_{BB} + W_\alpha V_{AB} + R_\alpha V_{AA}] = z[cS\omega + cV_{AA} + (1-c)V_{BB} + V_{AB}]$$

$$\text{for a } B_\alpha\text{-}A_\beta \text{ exchange} . \quad (11b)$$

In these expressions it has not been used that site i and site j are nearest-neighbors, since pair correlations are ignored in the Bragg-Williams approximation. This leads to

$$\frac{\Gamma_{\beta\alpha}}{\Gamma_{\alpha\beta}} = \frac{\exp\left[\frac{zcS\omega}{kT}\right] + \gamma}{\exp\left[-\frac{zcS\omega}{kT}\right] + \gamma} \quad (12)$$

with

$$\gamma = \frac{r}{1-r} \exp\left[\frac{E_s - E_0}{kT}\right] , \quad (13)$$

where $E_0 = z[cV_{AA} + (1-c)V_{BB} + V_{AB}]$. A combination of Eqs. (10) and (12) gives the following equation for the long-range order parameter:[6]

$$\frac{1-c+S+cS^2}{1-c-S+cS^2} = \frac{\exp\left[\frac{zcS\omega}{kT}\right] + \gamma}{\exp\left[-\frac{zcS\omega}{kT}\right] + \gamma} . \quad (14)$$

For $\gamma = 0$ this equation is equivalent with the solution obtained by free-energy extremization.[14] For $\gamma = 0$ one obtains an order-disorder transition temperature of $kT_c/\omega = zc(1-c)$.

It is interesting to relate the parameter γ to the number of ballistic exchanges per time unit. In Sec. II B 2 it was shown that the thermal-exchange attempt frequency is $\Gamma_t = \nu(1-r)$ and the ballistic-exchange frequency is $\Gamma_b = \nu r$. It follows that

$$\gamma = \frac{\Gamma_b}{\Gamma_t} \exp\left[\frac{E_s - E_0}{kT}\right] , \quad (15)$$

i.e., the parameter γ is proportional to the number of ballistic exchanges per time unit.

2. *Pair approximation*

In the pair approximation a microscopic configuration is specified by two parameters: S and Q [Eqs. (2) and (3)]. Let us consider an A_α-B_β exchange. Both the A atom and the B atom have $(z-1)$ unspecified neighbors. The statistical probability that the A atom is surrounded by an $A_i B_{z-1-i}$ cluster and the B atom by an $A_j B_{z-1-j}$ cluster is given by

$$P_{\alpha\beta}(i,j) = \left[\frac{Q_{AA}}{zR_\alpha}\right]^i \left[\frac{Q_{AB}}{zR_\alpha}\right]^{z-1-i} \begin{bmatrix} z-1 \\ i \end{bmatrix} \left[\frac{Q_{AB}}{zR_\beta}\right]^j \left[\frac{Q_{BB}}{zR_\beta}\right]^{z-1-j} \begin{bmatrix} z-1 \\ j \end{bmatrix} , \quad (16)$$

where the notation

$$\begin{bmatrix} n \\ k \end{bmatrix} = \frac{n!}{k!(n-k)!}$$

for the binominal coefficients has been used. For a B_α-A_β exchange the statistical probability that the B atom is surrounded by an $A_i B_{z-1-i}$ cluster and the A atom by an $A_j B_{z-1-j}$ cluster is

$$P_{\beta\alpha}(i,j) = \left[\frac{Q_{BA}}{zW_\alpha}\right]^i \left[\frac{Q_{BB}}{zW_\alpha}\right]^{z-1-i} \begin{bmatrix} z-1 \\ i \end{bmatrix} \left[\frac{Q_{AA}}{zW_\beta}\right]^j \left[\frac{Q_{BA}}{zW_\beta}\right]^{z-1-j} \begin{bmatrix} z-1 \\ j \end{bmatrix} . \quad (17)$$

The average exchange frequencies (or rather, the average exchange probabilities per unit time) can be written as weighted averages of the transition probability per unit time in Eq. (7) (with $\nu=1$):

$$\Gamma_{\alpha\beta}=\sum_{i=0}^{z-1}\sum_{j=0}^{z-1}P_{\alpha\beta}(i,j)\left[r+(1-r)\exp\left[-\frac{E_s-E_{\alpha\beta}(i,j)}{kT}\right]\right], \tag{18a}$$

$$\Gamma_{\beta\alpha}=\sum_{i=0}^{z-1}\sum_{j=0}^{z-1}P_{\beta\alpha}(i,j)\left[r+(1-r)\exp\left[-\frac{E_s-E_{\beta\alpha}(i,j)}{kT}\right]\right], \tag{18b}$$

with $E_{\alpha\beta}(i,j)=2V_{AB}+iV_{AA}+(z-1-i+j)V_{AB}+(z-1-j)V_{BB}$ and $E_{\beta\alpha}(i,j)=E_{\alpha\beta}(j,i)$. One can write the following rate equations:

$$\begin{aligned}\frac{d(R_\alpha\frac{1}{2}N)}{dt}&=-\Gamma_{\alpha\beta}\frac{Q_{AB}}{z}+\Gamma_{\beta\alpha}\frac{Q_{BA}}{z}\\&=-\frac{Q_{AB}}{z}\left[r+(1-r)\sum_{i=0}^{z-1}\sum_{j=0}^{z-1}P_{\alpha\beta}(i,j)\exp\left[-\frac{E_s-E_{\alpha\beta}(i,j)}{kT}\right]\right]\\&\quad+\frac{Q_{BA}}{z}\left[r+(1-r)\sum_{i=0}^{z-1}\sum_{j=0}^{z-1}P_{\beta\alpha}(i,j)\exp\left[-\frac{E_s-E_{\beta\alpha}(i,j)}{kT}\right]\right],\end{aligned} \tag{19a}$$

$$\begin{aligned}\frac{d(Q\frac{1}{2}N)}{dt}&=\frac{Q_{AB}}{z}\sum_{i=0}^{z-1}\sum_{j=0}^{z-1}(j-i)P_{\alpha\beta}(i,j)\left[r+(1-r)\exp\left[-\frac{E_s-E_{\alpha\beta}(i,j)}{kT}\right]\right]\\&\quad+\frac{Q_{BA}}{z}\sum_{i=0}^{z-1}\sum_{j=0}^{z-1}(i-j)P_{\beta\alpha}(i,j)\left[r+(1-r)\exp\left[-\frac{E_s-E_{\beta\alpha}(i,j)}{kT}\right]\right]\\&=\frac{Q_{AB}}{z}\left[r(z-1)\left[\frac{Q_{AB}}{zR_\beta}-\frac{Q_{AA}}{zR_\alpha}\right]+(1-r)\sum_{i=0}^{z-1}\sum_{j=0}^{z-1}(j-i)P_{\alpha\beta}(i,j)\exp\left[-\frac{E_s-E_{\alpha\beta}(i,j)}{kT}\right]\right]\\&\quad+\frac{Q_{BA}}{z}\left[r(z-1)\left[\frac{Q_{BA}}{zW_\alpha}-\frac{Q_{AA}}{zW_\beta}\right]+(1-r)\sum_{i=0}^{z-1}\sum_{j=0}^{z-1}(i-j)P_{\beta\alpha}(i,j)\exp\left[-\frac{E_s-E_{\beta\alpha}(i,j)}{kT}\right]\right].\end{aligned} \tag{19b}$$

Steady-state values of S and Q are given by the set of equations $d(R_\alpha\frac{1}{2}N)/dt\equiv\frac{1}{2}Nc(dS/dt)=0$ and $\frac{1}{2}N(dQ/dt)=0$. We note that the double sums in Eqs. (18) and (19) are easily performed analytically, using the mathematical relations

$$(x+y)^{z-1}=\sum_{i=0}^{z-1}x^iy^{z-1-i}\begin{bmatrix}z-1\\i\end{bmatrix}, \tag{20}$$

$$(z-1)x(x+y)^{z-2}=\sum_{i=0}^{z-1}ix^iy^{z-1-i}\begin{bmatrix}z-1\\i\end{bmatrix}. \tag{21}$$

Simple algebra shows that the steady-state equations (19) for $r=0$ are equivalent with the equations obtained by free-energy extremization in the pair approximation:[14]

$$\frac{Q_{AB}Q_{BA}}{Q_{AA}Q_{BB}}=\exp\left[\frac{\omega}{kT}\right], \tag{22a}$$

$$\left[\frac{Q_{AB}}{Q_{BA}}\right]^z=\left[\frac{R_\alpha R_\beta}{W_\alpha W_\beta}\right]^{z-1}. \tag{22b}$$

To prove this equivalence it is convenient to write Eqs. (19) and (22) in terms of the variables $P_{ij}=Q_{ij}\exp(V_{ij}/kT)$ with $i,j=A,B$, and show that Eqs. (19) imply the following equation:

$$\begin{aligned}&2[(P_{AA}P_{BB})^2-(P_{AB}P_{BA})^2]\\&\quad+[P_{AA}P_{BB}-P_{AB}P_{BA}](P_{AA}+P_{BB})(P_{AB}+P_{BA})=0.\end{aligned}$$

The critical temperature for $r=0$ is given by

$$\frac{kT_c}{\omega}=1/\ln\left[\frac{4z^2c(1-c)}{(z-2)^2-z^2(1-2c)^2}\right]. \tag{23}$$

For $r=0$, the kinetic approach of the pair approximation given in this section is similar to the treatment of Fultz.[15]

D. Monte Carlo simulations

Monte Carlo simulations of the model described in Secs. II A and II B were performed on a system of $8\times8\times8$ bcc unit cells (containing 1024 lattice sites) with periodic boundary conditions. We used a concentration of $c=0.5$, and $V_{AA}=V_{BB}=2V_{AB}$. The transition probability defined by Eq. (7) was employed. The algorithm consists of a repetition of the following steps: (i) choose randomly a lattice site, (ii) choose randomly one of the eight neighboring sites, and (iii) swap the atoms at the two selected sites if they are not of the same type and if a random number between zero and one is smaller than the transition probability (7) (with $\nu=1$). "Time" is measured in Monte Carlo steps (MCS) per atom: 1 MCS per atom corresponds to one exchange attempt per atom.

For temperatures $kT/\omega \geq 0.7$, a simulation of a steady state consisted of 10 000 MCS per atom (2000 MCS per atom for equilibration not included). For temperatures $kT/\omega < 0.7$, a simulation consisted of 25 000 MCS per atom (5000 MCS per atom not included).

To locate an order-disorder transition we proceed as follows. A starting value of the temperature T and the parameter γ (or r) is chosen, and a simulation is performed to obtain the value of the order-parameter S [through the relation $S = |R_\alpha - W_\beta|/(2c)$]. The final configuration of atoms is then used for a next simulation with slightly higher (or lower) value of either T or γ. Repeating this several times, the system can "go through" the transition, with order-parameter S changing from a value close to one to a value close to zero. Owing to finite-size effects, the transition at the higher temperatures is observed as a smooth s-shaped curve in an S-T or S-γ plot. In these cases we located the transition at the point of inflexion.

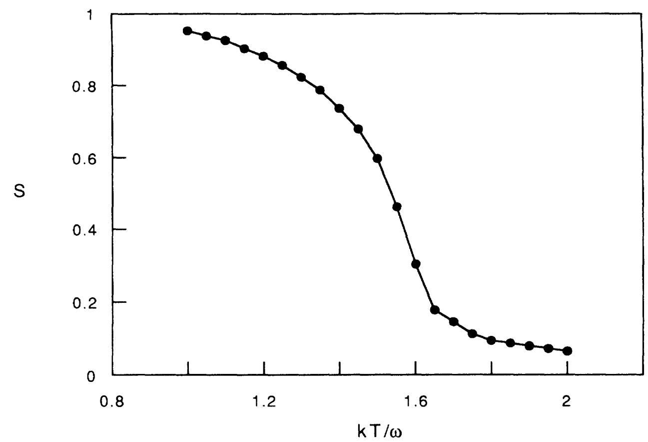

FIG. 2. Long-range order parameter S as a function of temperature kT/ω for zero irradiation, as determined by Monte Carlo simulation.

E. Phase diagram

1. T-c phase-diagram at $\gamma = 0$

For zero radiation ($r = 0$ or $\gamma = 0$) the mean-field approximations described in Sec. II C yield analytical expressions for the transition temperature as a function of composition. The phase diagram predicted by the Bragg-Williams approximation and the pair approximation is shown in Fig. 1. From a Monte Carlo simulation at $r = 0$ we estimate $kT_c/\omega = 1.6$ at $c = 0.5$ (the critical point was identified with the inflexion point in the S-T curve, see Fig. 2).

2. T-γ phase-diagram at $c = 0.5$ ($V_{AA} = V_{BB} = 2V_{AB}$)

In the Bragg-Williams approximation or the pair approximation, the T-γ phase diagram at fixed concentration $c = 0.5$ can be determined as follows. In the Bragg-Williams approximation one can solve the equation $d(R_\alpha \frac{1}{2}N)/dt \equiv \frac{1}{2}Nc(dS/dt) = 0$ by iteration with $S_{n+1} = S_n + (dS/dt)\delta t$, where δt is a parameter. In the pair approximation one can solve the two equations $\frac{1}{2}Nc(dS/dt) = 0$ and $\frac{1}{2}N(dQ/dt) = 0$ by iteration with $S_{n+1} = S_n + (dS/dt)\delta t$ and $Q_{n+1} = Q_n + (dQ/dt)\delta t$.

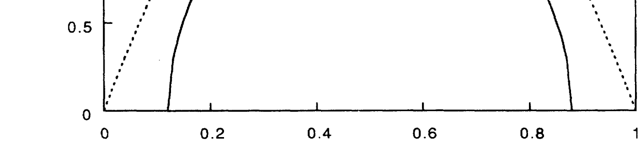

FIG. 1. Equilibrium phase diagram (zero radiation) in the Bragg-Williams (dashed curve) and the pair approximation (solid curve).

Below a tricritical temperature T_{tr}, the transition becomes first order, as observed by the occurrence of hysteresis loops (see Fig. 3). To obtain the lower branch of the hysteresis loops in Fig. 3(a) (Bragg-Williams approximation) and Fig. 3(b) (pair approximation), we used $S_0 = 10^{-5}$ as starting value for an iteration. If instead $S = 0$ is used, the system will remain at $S = 0$, since this corresponds to an (unstable) stationary state. Figure 3(c) shows a hysteresis loop obtained by Monte Carlo simulation at temperature $kT/\omega = 0.25$. With increasing temperature, the width of Monte Carlo loops is found to decrease, but it is difficult to locate sharply a tricritical temperature above which the hysteresis vanishes (since slow kinetics at low temperature also causes a small hysteresis at a second-order transition).

It should be emphasized that there is a fundamental difference between a mean-field hysteresis loop and a Monte Carlo hysteresis loop. Going through a mean-field loop corresponds to a system that remains in the same (ordered or disordered) phase as long as this phase is stable *or metastable*. This means that in the γ interval covered by a mean-field loop two stationary states exist, which are locally stable in configuration space. In contrast, in a Monte Carlo simulation the system can escape from a metastable state *before* this state becomes unstable, by overcoming the barrier required to reach the stationary stable state (i.e., the state with lower generalized free energy; the concept of generalized free energy is discussed by Bellon and Martin[6]). This implies that the γ interval covered by a Monte Carlo loop is smaller than the interval of bistability.

In Fig. 4 the T-γ phase diagram is shown. The region of bistability (indicated as two diverging curves) is significantly smaller in the pair approximation than in the Bragg-Williams approximation. Monte Carlo results are represented by dots, and hysteresis at low temperature is indicated by two separate dots. The solution in

TABLE I. Estimated values of the tricritical temperature, below which hysteresis is observed [the Bragg-Williams value $T_{tr}/T_c = 2/(3+\sqrt{3}) \approx 0.4226$ is exact (Ref. 6)].

	T_{tr}/T_c
Bragg-Williams approximation	0.4226
Pair approximation	0.33
Monte Carlo simulation	0.23±0.03

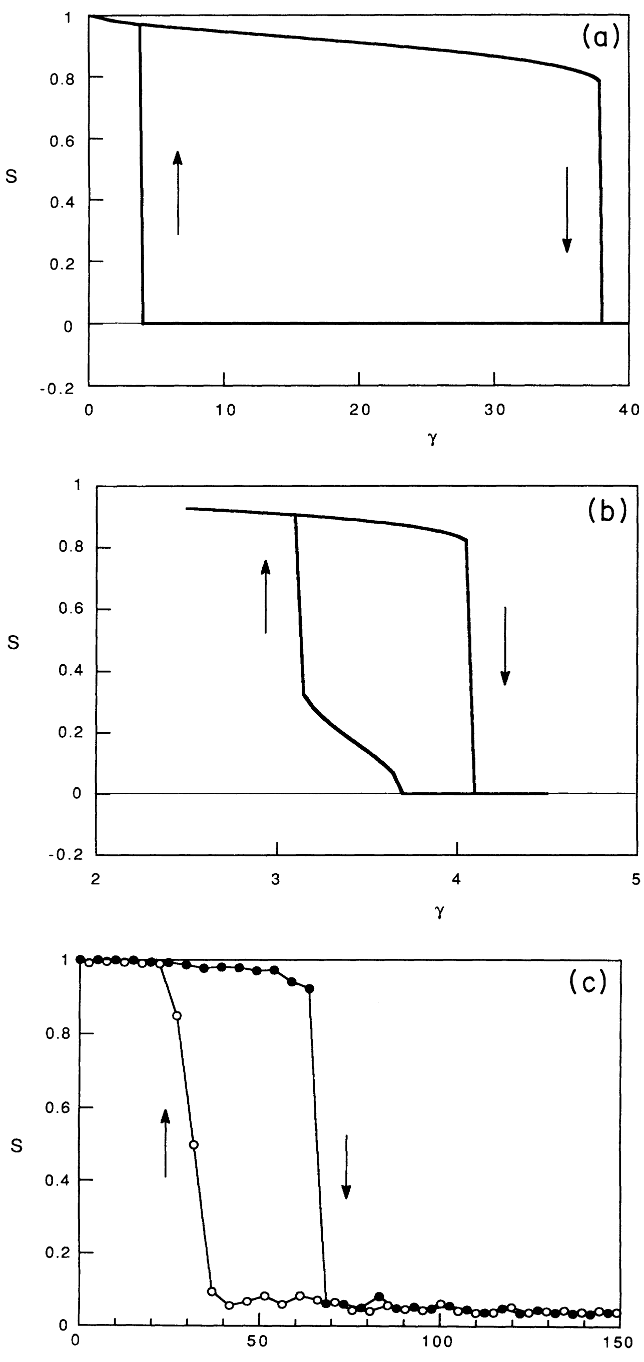

FIG. 3. (a) Hysteresis loop at $kT/\omega = 0.4$ (Bragg-Williams approximation). (b) Hysteresis loop at $kT/\omega = 0.4$ (pair approximation). (c) Hysteresis loop at $kT/\omega = 0.25$ (Monte Carlo simulation).

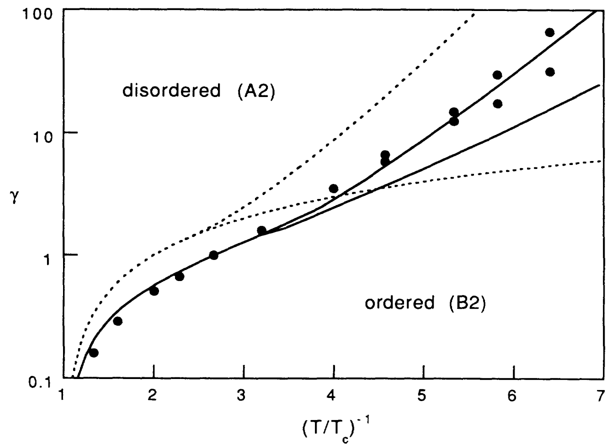

FIG. 4. Dynamical phase diagram at $c = 0.5$, in the Bragg-Williams approximation (dashed curves), in the pair approximation (solid curves), and from Monte Carlo simulations (dots). Here T_c is the order-disorder temperature for $\gamma = 0$.

the pair approximation is in excellent agreement with the Monte Carlo results. Apparently, the pair approximation works rather well for the bcc structure.[16] Estimated values of the tricritical temperature are given in Table I.

F. Finite-size and finite-time effects in simulations

In a Monte Carlo simulation of an order-disorder transition in a system of a few thousand atoms, finite-size effects occur. Figure 5 demonstrates the effect of system size on the first-order transition at low temperature. The hysteresis loop for a system of $15 \times 15 \times 15$ unit cells (containing 6750 atoms) is shifted to lower values of γ with respect to the loop for a system of $8 \times 8 \times 8$ unit cells (containing 1024 atoms).

Figure 5 also demonstrates the effect on a Monte Carlo hysteresis loop of the time spent at a single (S, γ) point of the curve. Increasing this time from 25 000 MCS

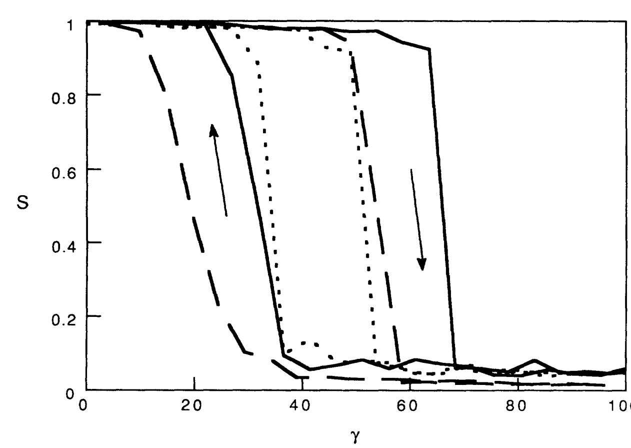

FIG. 5. Monte Carlo hysteresis loops at $kT/\omega = 0.25$. Solid curves: system of $8 \times 8 \times 8$ unit cells, using 5000+25 000 MCS [see Fig. 3(c)]. Broken curves: $15 \times 15 \times 15$ unit cells and 5000+25 000 MCS. Dashed curves: $8 \times 8 \times 8$ unit cells and 15 000+75 000 MCS.

(+5000 MCS for equilibration) to 75 000 MCS (+15 000 MCS for equilibration), narrows the loop significantly.

III. RADIATION-INDUCED REPLACEMENT COLLISION SEQUENCES

The effect of radiation on the state of order of a binary alloy depends on the type of alloy, but also on the nature of the radiation. There is experimental evidence,[3] that energetic electrons produce ballistic displacements of a few atoms, whereas fast neutrons and heavy ions can produce so-called replacement collision sequences (RCS) of many atoms, leading to the occurrence of cascades in the alloy. Replacement collision sequences are studied in this section, by modifying the model presented in the previous section.

A. Model

We consider replacement collision sequences in the [111] direction (with alternating α and β sites), and we assume that all sequences are of the same length $2b$ (b is a positive integer). For simplicity, the atom knocked from the final site is reinserted at the vacancy created at the first site of the sequence, to avoid the formation of vacancies and interstitials. Thus an RCS is considered as a cyclic permutation of $2b$ atoms on a straight line (in Sec. III E we study closed loops).

We will investigate the effect of the sequence length $2b$ on the T-γ phase diagram.

The dynamics of the system is no longer given by Eq. (7), but is modified as follows. Each atom has a probability per unit time of 1-r to attempt a thermal exchange with one of its neighbors, and a probability per unit time of r to be the starting point of an RCS of length $2b$. Thermal exchanges have a transition probability per unit time given by Eq. (6) (with $\nu=1$).

B. Mean-field solutions

1. Bragg-Williams approximation

In this section it is demonstrated that the Bragg-Williams equation (14) for the long-range order parameter S is independent of the sequence length $2b$, if one appropriately generalizes the definition (13) of the parameter γ. This implies that the T-γ phase diagram for $b=1$ is the same as for $b>1$, in the Bragg-Williams approximation.

Equation (14) was derived from the rate equation (8) for the total number $R_\alpha \frac{1}{2}N$ of A_α atoms in the lattice. The average effect of a single RCS of length $2b$ on the number $R_\alpha \frac{1}{2}N$ is easily evaluated, in the Bragg-Williams approximation:

$$\Delta(R_\alpha \tfrac{1}{2}N)=b(W_\beta-R_\alpha)=b(W_\alpha W_\beta-R_\alpha R_\beta)\ , \tag{24}$$

since each A_β atom in an RCS raises the number $R_\alpha \frac{1}{2}N$ by one, and each A_α atom lowers the number $R_\alpha \frac{1}{2}N$ by one. The second step in Eq. (24) follows directly from the definitions (2). Using Eq. (24) in Eq. (8) leads to Eq. (14) with the following generalized definition of the parameter γ:

$$\gamma=b\frac{r}{1-r}\exp\left[\frac{E_s-E_0}{kT}\right] \tag{25}$$

which reduces to Eq. (13) for $b=1$. Since the number of ballistically displaced pairs of atoms per time unit is $\Gamma_b=br$ and the thermal-exchange attempt frequency is $\Gamma_t=(1-r)$, Eq. (25) can be written as

$$\gamma=\frac{\Gamma_b}{\Gamma_t}\exp\left[\frac{E_s-E_0}{kT}\right]. \tag{26}$$

This equation is identical with Eq. (15). The number of ballistically displaced atoms per time unit can be specified either by the two parameters b and r or by the single parameter γ.

2. Pair approximation

In this section we show how the two rate equations (19a) and (19b), corresponding to the pair approximation, have to be modified for the case where replacement collision sequences occur. The derivation is restricted to $b>>1$, i.e., long replacement sequences. Hence, one can assume that an arbitrary RCS contains bR_α A_α atoms and bW_β A_β atoms. It follows immediately that the only modification of Eq. (19a) is the inclusion of a factor b in the two terms proportional to r [using Eq. (24) and the identity $Q_{BA}-Q_{AB}=z(W_\beta-R_\alpha)$].

To evaluate the modification of Eq. (19b), we will determine the average effect of an RCS on the number $Q\frac{1}{2}N$ of A-A bonds. The effect of displacing (along the RCS) an A_α atom to a neighboring β site, is that

$$(z-2)\frac{Q_{AA}}{zR_\alpha}$$

A-A bonds are broken upon leaving the α site, and

$$(z-2)\left[\frac{Q_{AA}Q_{AA}}{zR_\alpha zW_\beta}+\frac{Q_{AB}Q_{AB}}{zR_\alpha zR_\beta}\right]$$

A-A bonds are created upon arrival at the β site. The factor z-2 instead of z accounts for the fact that no bonds within the RCS are created or broken by cyclic permutation, except at the first and the last sites. Since the RCS is assumed to be long, the error introduced at the fist and the last sites can be neglected. Analogous expressions hold for the displacement of an A_β atom. This leads to the following expression for the average effect of a single RCS on the number $Q\frac{1}{2}N$ of A-A bonds:

$$\begin{aligned}\Delta(Q\tfrac{1}{2}N)&=(z-2)bR_\alpha\left[-\frac{Q_{AA}}{zR_\alpha}+\frac{Q_{AA}Q_{AA}}{zR_\alpha zW_\beta}+\frac{Q_{AB}Q_{AB}}{zR_\alpha zR_\beta}\right]+(z-2)bW_\beta\left[-\frac{Q_{AA}}{zW_\beta}+\frac{Q_{AA}Q_{AA}}{zW_\beta zR_\alpha}+\frac{Q_{BA}Q_{BA}}{zW_\beta zW_\alpha}\right]\\&=\frac{Q_{AB}}{z}(z-2)b\left[\frac{Q_{AB}}{zR_\beta}-\frac{Q_{AA}}{zR_\alpha}\right]+\frac{Q_{BA}}{z}(z-2)b\left[\frac{Q_{BA}}{zW_\alpha}-\frac{Q_{AA}}{zW_\beta}\right].\end{aligned} \tag{27}$$

Thus, the only modification of Eq. (19b) is the inclusion of a factor $b(z-2)/(z-1)$ in the two terms proportional to r.

The modified rate equations for $b>>1$ correspond to a T-γ phase diagram that depends on the value of b. However, if one uses the generalized definition (25) for γ (so that γ is a measure of the number of ballistically displaced atoms per time unit), this b dependence turns out to be negligibly small.

C. Monte Carlo simulations

For the simulation of a system with both replacement collision sequences and thermally activated exchanges, the following modification of the Monte Carlo method described in Sec. II D must be made: for each transition, a random number is compared with the parameter r, to decide whether a replacement sequence or a thermal exchange [with acceptance probability given by Eq. (6)] is going to take place.

A rather subtle point should be mentioned here. We found numerically, that for $b=1$ the ensemble average of the long-range order parameter S is independent of the order of selecting the atoms for a transition, whereas for $b>1$ a regular order of selection gives a slightly different result than a random order gives. Hence, to model an alloy under radiation as realistically as possible, we used a random order of selection.

D. Phase diagram for $b \gg 1$

In Fig. 6 the T-γ phase diagram in pair approximation is shown, both for $b=1$ and for $b>>1$. The major effect of going from $b=1$ to $b>>1$ is the disappearance of the region of bistability. In other words, while the transition for $b=1$ becomes first order below a tricritical temperature, the transition for $b>>1$ remains second order. Figure 7 demonstrates this, by a hysteresis S-γ loop for $b=1$, and a reversible curve for $b>>1$ at the same temperature.

These results can be compared with Monte Carlo simulations for $b=5$. Figures 8(a) and 8(b) compare the tran-

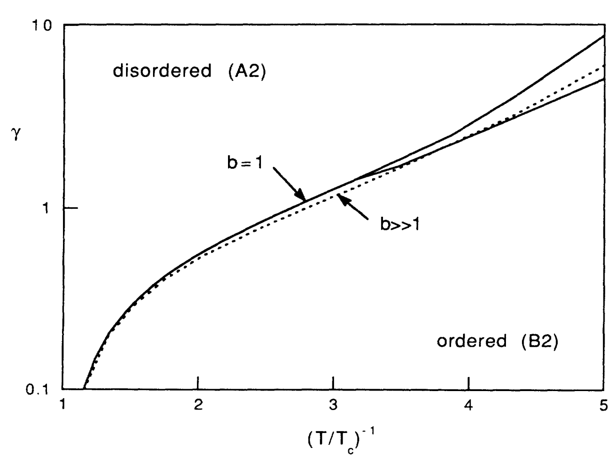

FIG. 6. Phase diagram in the pair approximation, for $b=1$ (solid curves) and $b \gg 1$ (dashed curve).

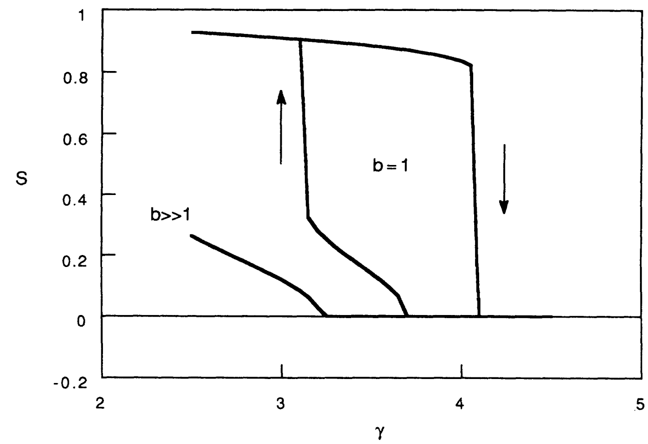

FIG. 7. The transition at $kT/\omega=0.4$ in the pair approximation shows hysteresis for $b=1$, and is reversible for $b \gg 1$.

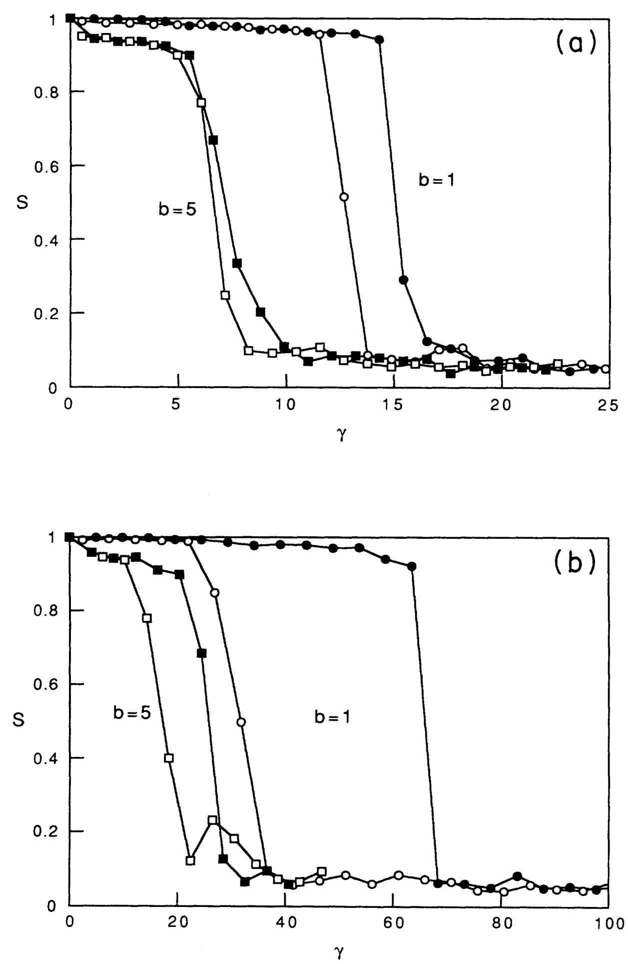

FIG. 8. (a) Transition at $kT/\omega=0.3$, by Monte Carlo simulation, for $b=1$ (circles) and $b=5$ (squares). Solid symbols: increasing γ, open symbols: decreasing γ. (b) Transition at $kT/\omega=0.25$, by Monte Carlo simulation, for $b=1$ (circles) and $b=5$ (squares). Solid symbols: increasing γ, open symbols: decreasing γ.

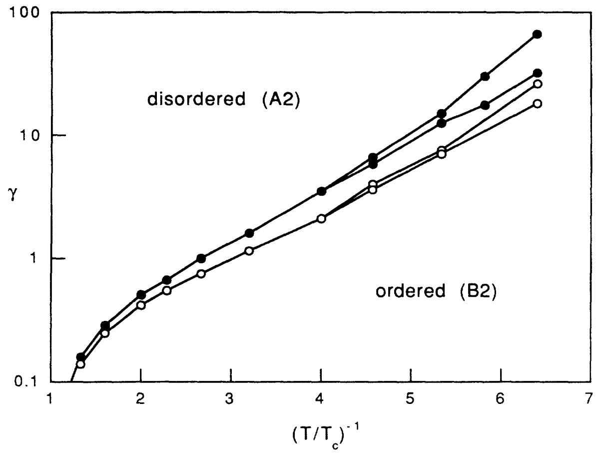

FIG. 9. Phase diagram by Monte Carlo simulation, for $b=1$ (solid circles) and $b=5$ (open circles).

sitions for $b=1$ and $b=5$, at temperatures $kT/\omega=0.3$ and $kT/\omega=0.25$. Although kinetics might play a minor role here, the hysteresis width at $b=5$ is significantly reduced, in agreement with the disappearance of hysteresis in the pair approximation for $b>>1$. Figure 9 compares the Monte Carlo phase diagrams for $b=1$ and $b=5$. In addition to the reduced hysteresis (which is consistent with the stochastic treatment of Ref. 6), one observes a shift of the transition toward lower values of the parameter γ or the temperature T. This is in qualitative agreement with the shift of the transition in pair approximation (Fig. 6).

E. Replacement collision loops

In radiation-induced cascades one may find replacement sequences in the form of closed loops instead of straight lines.[1,17,18] We performed some simulations of rectangular replacement loops with [111] sides, for $b=5$ (rectangles with sides of length 3 and 4 nearest-neighbor distances) and for $b=10$ (rectangles with sides of length 6 and 8 nearest-neighbor distances), at temperatures $kT/\omega=0.5$, 0.4, and 0.25. The orientation of a rectangle was chosen at random. The results turned out to be indistinguishable from the results for straight replacement sequences. This means that the γ-T phase diagram for rectangular loops with $b=5$ and $b=10$ is the same as for straight replacement sequences with $b=5$ (Fig. 9).

IV. SUBTHRESHOLD RADIATION

In this section a realistic treatment of subthreshold irradiation is given. Subthreshold radiation has an energy too low to induce direct displacements of atoms, and therefore enhances atomic transport only through a vacancy mechanism.

A. Model

We consider a binary bcc A/B alloy with a small concentration of vacancies, which is in fact a ternary system. Vacancies are denoted by the symbol X, and are assumed to be noninteracting, i.e., $V_{AX}=V_{BX}=V_{XX}=0$ (however, vacancies interact indirectly through interaction between A and B atoms).

There are 15 variables in the pair approximation: six point variables (the sublattice occupancies R_α, W_α, X_α, R_β, W_β, X_β) and nine pair variables (the pair probabilities Q_{AA}, Q_{AB}, Q_{AX}, Q_{BA}, Q_{BB}, Q_{BX}, Q_{XA}, Q_{XB}, Q_{XX}). The number of independent variables is smaller than 15. For simplicity we restrict ourselves to the symmetric case: $c_A=c_B\equiv c$ and $V_{AA}=V_{BB}=2V_{AB}$. This reduces the number of independent variables to four.[19] These four variables, S, Q, Q_1, and Q_2, are defined through

$$\begin{aligned} &R_\alpha=R_\beta=c(1+S)\ , \\ &W_\alpha=W_\beta=c(1-S)\ , \\ &X_\alpha=X_\beta=1-2c\ ; \end{aligned} \tag{28}$$

$$\begin{aligned} &Q_{AA}=Q_{BB}=Q,\quad Q_{AB}=zR_\alpha-Q-Q_1\ , \\ &Q_{BA}=zW_\beta-Q-Q_2,\quad Q_{AX}=Q_{XB}=Q_1\ , \\ &Q_{XA}=Q_{BX}=Q_2,\quad Q_{XX}=zX_\alpha-Q_1-Q_2\ . \end{aligned} \tag{29}$$

The concentration c is fixed by the value of the vacancy concentration c_x, through the relation $2c+c_x=1$. This value ranges from typically 10^{-5} in thermal equilibrium, to nearly 10^{-2} under high radiation flux.[20] Fortunately, steady-state solutions of rate equations (these are described below) turn out to have a negligible dependence on the value of c_x in the range 10^{-5}–10^{-2}. Therefore, we chose a fixed value of $c_x=10^{-3}$. We verified that the γ-T phase diagrams for $c_x=10^{-3}$ and $c_x=10^{-4}$ are indistinguishable on the scale of interest here.

B. Dynamics

We assume that the dynamics takes place through atom-vacancy exchanges. Thus, both thermal and forced atom-vacancy exchanges occur.

For the transition probability per unit time we use the function (see Sec. II B)

$$W(A_iX_j\to X_iA_j)=\nu\left[r+(1-r)\exp\left[-\frac{E_s'-\sum_{i'}V_{ii'}}{kT}\right]\right]\ , \tag{30}$$

for an A_i-X_j exchange. Here E_s' is a constant. A similar expression holds for a B-X exchange. Again, we choose the unit of time as $\tau=1/\nu$, i.e., we set $\nu=1$.

C. Mean-field solutions

In Sec. II it was demonstrated that the pair approximation works rather well for a lattice model with two types of competing dynamics. Therefore, we rely on the pair approximation in this section. For completeness we also give the solution in the point approximation.

1. Bragg-Williams approximation

In the Bragg-Williams approximation a microscopic configuration of the system is specified by a single parameter: the long-range order parameter S [see Eq. (28)]. One can write the following rate equation for the total number of A atoms at the α sublattice:

$$\frac{d(R_\alpha \frac{1}{2}N)}{dt} = -\Gamma_{\alpha\beta}^{AX} R_\alpha X_\beta + \Gamma_{\beta\alpha}^{AX} W_\beta X_\alpha \, , \tag{31}$$

where $\Gamma_{\alpha\beta}^{AX}$ and $\Gamma_{\beta\alpha}^{AX}$ are the $A_\alpha - X_\beta$ and $A_\beta - X_\alpha$ exchange frequencies, respectively. These frequencies (or rather, average exchange probabilities per unit time) are obtained by applying the Bragg-Williams approximation in Eq. (30) (using $V_{AA} = V_{BB}$ and $\nu = 1$):

$$\Gamma_{\alpha\beta}^{AX} = r + (1-r)\exp\left[\frac{E_0' - E_s'}{kT}\right]\exp\left[-\frac{zcS\omega}{2kT}\right] , \tag{32a}$$

$$\Gamma_{\beta\alpha}^{AX} = r + (1-r)\exp\left[\frac{E_0' - E_s'}{kT}\right]\exp\left[\frac{zcS\omega}{2kT}\right] , \tag{32b}$$

with $E_0' = zc(V_{AA} + V_{AB})$. Steady-state solutions of Eq. (31) are given by

$$\frac{1+S}{1-S} = \frac{\exp\left[\dfrac{zcS\omega}{2kT}\right] + \gamma}{\exp\left[-\dfrac{zcS\omega}{2kT}\right] + \gamma} \tag{33}$$

with

$$\gamma = \frac{r}{1-r}\exp\left[\frac{E_s' - E_0'}{kT}\right] . \tag{34}$$

For $r = \gamma = 0$, Eq. (33) is identical with Eq. (14) for the Bragg-Williams steady-state solution for a direct transport mechanism. This implies that the critical temperature for $r = \gamma = 0$ and $c_x \ll 1$ is $kT_c/\omega = 2$.

2. Pair approximation

In the pair approximation a microscopic configuration is specified by four parameters [see Eqs. (28) and (29)]. Let us consider and $A_\alpha - X_\beta$ exchange. Both the A atom and the vacancy X have (z-1) unspecified neighbors. The statistical probability that the A atom is surrounded by an $A_i B_j X_{z-1-i-j}$ cluster and the vacancy X by an $A_m B_n X_{z-1-m-n}$ cluster, is given by

$$P_{\alpha\beta}^{AX}(i,j,m,n) = \left[\frac{Q_{AA}}{zR_\alpha}\right]^i \left[\frac{Q_{AB}}{zR_\alpha}\right]^j \left[\frac{Q_{AX}}{zR_\alpha}\right]^{z-1-i-j} \begin{bmatrix} z-1 \\ i,j \end{bmatrix} \left[\frac{Q_{AX}}{zX_\beta}\right]^m \left[\frac{Q_{BX}}{zX_\beta}\right]^n \left[\frac{Q_{XX}}{zX_\beta}\right]^{z-1-m-n} \begin{bmatrix} z-1 \\ m,n \end{bmatrix} , \tag{35}$$

where the notation

$$\begin{bmatrix} k \\ i,j \end{bmatrix} = \frac{k!}{i!\,j!\,(k-i-j)!}$$

for a multinomial has been used. For an $X_\alpha - A_\beta$ exchange, the statistical probability that the A atom is surrounded by an $A_i B_j X_{z-1-i-j}$ cluster and the vacancy X by an $A_m B_n X_{z-1-m-n}$ cluster, is given by

$$P_{\beta\alpha}^{AX}(i,j,m,n) = \left[\frac{Q_{AA}}{zW_\beta}\right]^i \left[\frac{Q_{BA}}{zW_\beta}\right]^j \left[\frac{Q_{XA}}{zW_\beta}\right]^{z-1-i-j} \begin{bmatrix} z-1 \\ i,j \end{bmatrix} \left[\frac{Q_{XA}}{zX_\alpha}\right]^m \left[\frac{Q_{XB}}{zX_\alpha}\right]^n \left[\frac{Q_{XX}}{zX_\alpha}\right]^{z-1-m-n} \begin{bmatrix} z-1 \\ m,n \end{bmatrix} . \tag{36}$$

Analogous expressions hold for $P_{\alpha\beta}^{BX}(i,j,m,n)$ and $P_{\beta\alpha}^{BX}(i,j,m,n)$. One can write the following four rate equations:

$$\frac{d(R_\alpha \frac{1}{2}N)}{dt} = \sum_i \sum_j \sum_m \sum_n [Q_{XA} P_{\beta\alpha}^{AX}(i,j,m,n) - Q_{AX} P_{\alpha\beta}^{AX}(i,j,m,n)]\left[r + (1-r)\exp\left[\frac{iV_{AA} + jV_{AB} - E_s'}{kT}\right]\right] , \tag{37a}$$

$$\frac{d(Q_{AA} \frac{1}{2}N)}{dt} = \sum_i \sum_j \sum_m \sum_n (m-i)[Q_{XA} P_{\beta\alpha}^{AX}(i,j,m,n) + Q_{AX} P_{\alpha\beta}^{AX}(i,j,m,n)]\left[r + (1-r)\exp\left[\frac{iV_{AA} + jV_{AB} - E_s'}{kT}\right]\right] , \tag{37b}$$

$$\begin{aligned} \frac{d(Q_{AX} \frac{1}{2}N)}{dt} = {} & \sum_i \sum_j \sum_m \sum_n [Q_{XA} P_{\beta\alpha}^{AX}(i,j,m,n) - Q_{AX} P_{\alpha\beta}^{AX}(i,j,m,n)]\left[r + (1-r)\exp\left[\frac{iV_{AA} + jV_{AB} - E_s'}{kT}\right]\right] \\ & + \sum_i \sum_j \sum_m \sum_n [iQ_{XB} P_{\beta\alpha}^{BX}(i,j,m,n) - mQ_{BX} P_{\alpha\beta}^{BX}(i,j,m,n)]\left[r + (1-r)\exp\left[\frac{iV_{AB} + jV_{BB} - E_s'}{kT}\right]\right] , \end{aligned} \tag{37c}$$

$$\frac{d(Q_{BX}\frac{1}{2}N)}{dt}=\sum_i\sum_j\sum_m\sum_n[Q_{XB}P^{BX}_{\beta\alpha}(i,j,m,n)-Q_{BX}P^{BX}_{\alpha\beta}(i,j,m,n)]\left[r+(1-r)\exp\left[\frac{iV_{AB}+jV_{BB}-E'_s}{kT}\right]\right]$$
$$+\sum_i\sum_j\sum_m\sum_n[jQ_{XA}P^{AX}_{\beta\alpha}(i,j,m,n)-nQ_{AX}P^{AX}_{\alpha\beta}(i,j,m,n)]\left[r+(1-r)\exp\left[\frac{iV_{AA}+jV_{AB}-E'_s}{kT}\right]\right]. \tag{37d}$$

Summations in Eqs. (37) over i, j, m, and n run from 0 to z-1, and are subject to the conditions $i+j\leq z-1$ and $m+n\leq z-1$. They are easily performed analytically, using the mathematical relations

$$(x+y+z)^k=\sum_{i=0}^{k}\sum_{j=0}^{k}x^iy^jz^{k-i-j}\begin{bmatrix}k\\i,j\end{bmatrix}, \tag{38}$$

$$kx(x+y+z)^{k-1}=\sum_{i=0}^{k}\sum_{j=0}^{k}ix^iy^jz^{k-i-j}\begin{bmatrix}k\\i,j\end{bmatrix}, \tag{39}$$

with summations subject to the condition $i+j\leq k$.

Steady-state values of S, Q, Q_1, and Q_2 are obtained by solving the set of equations $d(R_\alpha\frac{1}{2}N)/dt=0$, $d(Q_{AA}\frac{1}{2}N)/dt=0$, $d(Q_{AX}\frac{1}{2}N)/dt=0$, and $d(Q_{BX}\frac{1}{2}N)/dt=0$. For $r=0$ and $c_x\ll 1$ it is straightforward to show that these equations imply the equilibrium equations (22), obtained by free-energy extremization in the pair approximation. For $r=0$ the kinetic approach of the pair approximation given in this section is similar to the treatment of Fultz.[15] Instead of the parameter r we will use the parameter γ_x defined as

$$\gamma_x=\frac{r}{1-r}\exp\left[\frac{E'_s}{kT}\right]. \tag{40}$$

D. Phase diagram

The Bragg-Williams phase diagram, as obtained by solving Eq. (31) using the iterative method of Sec. II E 2, is shown in Fig. 10, together with the phase diagram of Sec. II for a direct transport mechanism. For a vacancy mechanism, the transition becomes first order beyond a tricritical point at ($T_{tr}/T_c=\frac{1}{3}$, $\gamma_{tr}=2$) (this is derived in the way indicated in Ref. 6).

To obtain the phase diagram in the pair approximation, the four steady-state equations (37) have to be solved. We used four-dimensional Newton-Raphson iteration (since the iterative method of Sec. II E 2 gave no convergence). Below a tricritical temperature of $T_{tr}/T_c\approx 0.26$, the transition becomes first order, as demonstrated by the discontinuity in the long-range order parameter for $T/T_c=0.23$ in Fig. 11 (the critical temperature at $r=\gamma_x=0$ is $kT_c/\omega=1.737$ for vacancy concentration $c_x=10^{-3}$; cf. $kT_c/\omega=1.738$ for $c_x=0$). The discontinuous curve in Fig. 11 was obtained upon increasing the parameter γ_x. The lower branch of the hysteresis loop could not be determined by Newton-Raphson iteration, due to the fact that $S=0$ is a solution of Eqs. (37) for all values of γ_x. In Fig. 12 the phase diagram in the pair approximation is presented, together with the phase diagram of Sec. II for a direct transport mechanism. The broken curve for the vacancy mechanism represents the upper branch of the first-order hysteresis loop.

V. CONCLUSIONS

Ordering in binary bcc alloys under radiation has been studied by mean-field solutions and Monte Carlo simulations of dynamical lattice models. The simulations,

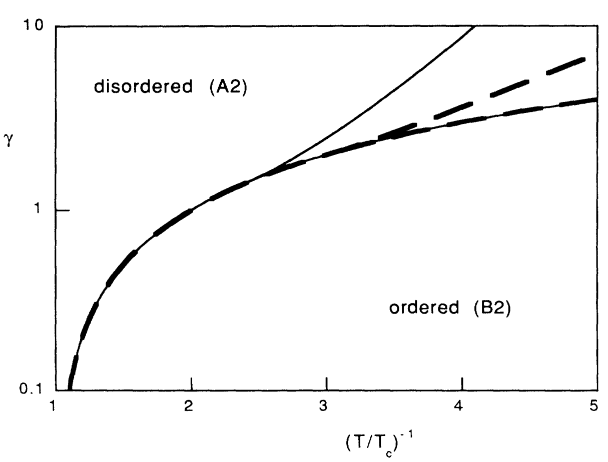

FIG. 10. Phase diagram in Bragg-Williams approximation, for vacancy mechanism (broken curve) and direct-exchange mechanism (solid curve).

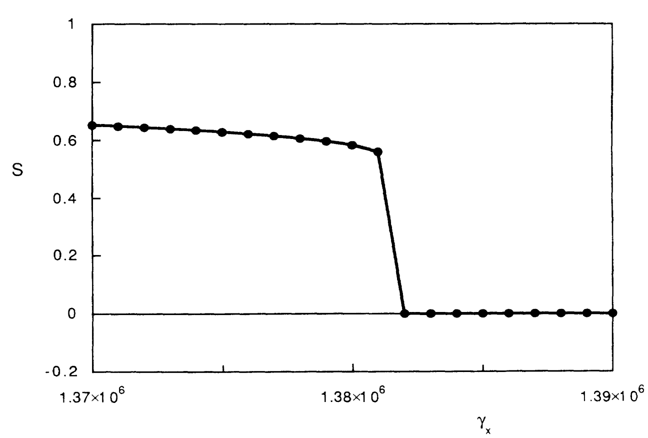

FIG. 11. First-order transition for vacancy mechanism in pair approximation, at temperature $kT/\omega=0.4$.

which yield in principle exact numerical results, demonstrate that the pair approximation works well for these models with competing dynamics.

A realistic treatment of subthreshold irradiation, with thermal and forced atom-vacancy exchanges, has been presented for an $A_{50}B_{50}$ alloy. The γ_x-T phase diagram has been determined. The $B2$ ordering transition becomes first order beyond a tricritical point. It is interesting to note, that the ferromagnetic Ising models with competing dynamics studied in Refs. 8 and 9 also have a phase transition that changes from second order to first order.

A simplified treatment of high-energy irradiation has been presented, using a model with a direct-exchange mechanism: thermal exchanges of two atoms and forced exchanges of two or more atoms. In the pair approximation, for forced exchanges of two atoms we found again a tricritical point, for forced exchanges of more than two atoms the transition is shifted towards lower temperatures, and for forced exchanges of many (say, ten) atoms the transition remains always second order. Monte Carlo simulations confirm the tricritical point for forced exchanges of two atoms and also the shift of the transition for exchanges of more than two atoms.

Finally, we repeat that a complete model for high-energy irradiation includes: thermally activated atomic jumps (via a vacancy mechanism and/or an interstitial mechanism), forced direct exchanges of two or more atoms, and also forced atom-vacancy exchanges due to secondary projectiles with subthreshold energy.[5] It is an open question, whether such a complete model yields significantly different results than the results presented in this paper.

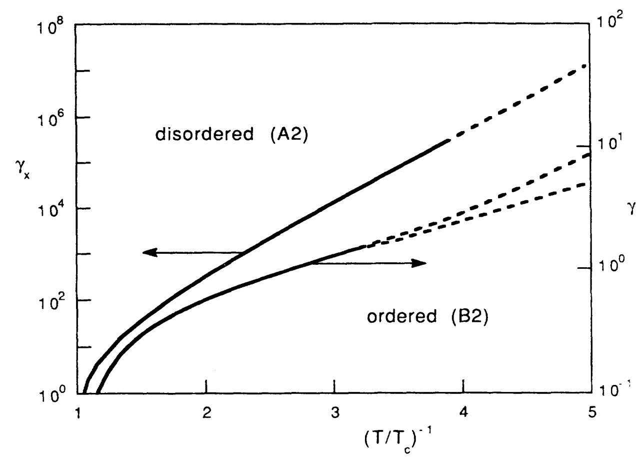

FIG. 12. Phase diagram in pair approximation for vacancy mechanism (upper curve) and direct-exchange mechanism (lower curve). Dashed curves indicate first-order transition.

*Present address: CECAM, Université de Paris-Sud, Bâtiment 506, 91405 Orsay CEDEX, France.

[1] J. B. Gibson, A. N. Goland, M. Milgram, and G. H. Vineyard, Phys. Rev. **120**, 1229 (1960).
[2] A. Tenenbaum and N. V. Doan, Philos. Mag. **35**, 379 (1977).
[3] E. M. Schulson, J. Nucl. Mater. **83**, 239 (1979).
[4] P. L. Garrido and J. Marro, Phys. Rev. Lett. **62**, 1929 (1989).
[5] P. Regnier, Ann. Chim. Fr. **9**, 49 (1984).
[6] P. Bellon and G. Martin, Phys. Rev. B **39**, 2403 (1989).
[7] F. Haider, in *Proceedings of European Workshop on Ordering and Disordering,* edited by A. R. Yavari (Elsevier, Amsterdam, 1992).
[8] J. M. Gonzalez-Miranda, P. L. Garrido, J. Marro, and J. L. Lebowitz, Phys. Rev. Lett. **59**, 1934 (1987).
[9] R. Dickman, Phys. Lett. A **122**, 463 (1987).
[10] S. Katz, J. L. Lebowitz, and H. Spohn, Phys. Rev. B **28**, 1655 (1983).
[11] P. L. Garrido, A. Labarta, and J. Marro, J. Stat. Phys. **49**, 551 (1987).
[12] K.-t. Leung, B. Schmittmann, and R. K. P. Zia, Phys. Rev. Lett. **62**, 1772 (1989).
[13] R. Dickman, Phys. Rev. A **41**, 2192 (1990).
[14] T. Muto and Y. Takagi, in *Solid State Physics,* Vol. 1, edited by F. Seitz and D. Turnbull (Academic, New York, 1955), pp. 194–282.
[15] B. Fultz, J. Mater. Res. **5**, 1419 (1990).
[16] R. Kikuchi and H. Sato, Acta Metal. **22**, 1099 (1974).
[17] A. Tenenbaum, Phys. Lett. **63A**, 155 (1977).
[18] N. V. Doan and Y. Adda, Philos. Mag. A **56**, 269 (1987).
[19] K. Gschwend, H. Sato, and R. Kikuchi, J. Chem. Phys. **69**, 5006 (1978).
[20] S. Banerjee and K. Urban, Phys. Status Solidi A **81**, 145 (1984).